Journal of Materials Chemistry C

Accepted Manuscript

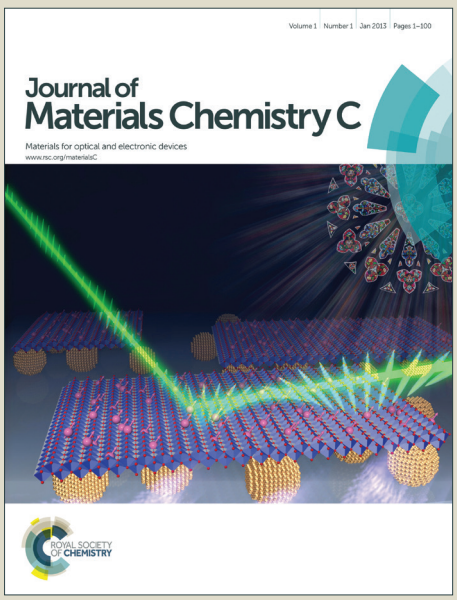

ROYAL SOCIETY OF CHEMISTRY

www.rsc.org/materialsC

Atypical multiferroicity of $HoCrO_3$ in bulk and film geometry†

A. Ghosh,[a] A. Pal,[a] K. Dey,[a] S. Majumdar[a] and S. Giri*[a]

Received Xth XXXXXXXXXX 20XX, Accepted Xth XXXXXXXXX 20XX
First published on the web Xth XXXXXXXXXX 200X
DOI: 10.1039/b000000x

We report ferroelectricity in antiferromagnetic $HoCrO_3$ with a reasonably large value of spontaneous electric polarization (~ 0.32 μC/cm^2 at 10 K) from the measurement of pyroelectric current. Appearance of ferroelectricity is further confirmed in the film geometry. Intriguingly, onset of polar order is observed at significantly higher temperature ($\sim$ 240 K) than the Néel temperature (T_N = 142 K). Survival of remanent polarization is confirmed from the electric polarization hysteresis loops above and below T_N for polycrystalline and film specimens. Structural analysis suggests that polar oxygen octahedral rotations and Ho displacements in the non-centrosymmetric $Pna2_1$ space group engineer ferroelectricity. The results indicate that occurrence of polar order in $HoCrO_3$ resembles neither the typical case of proper ferroelectrics nor the improper ferroelectrics.

1 Introduction

Occurrence of multiferroic order, that involves coexistence of more than one ferroic order parameters, has been currently recognised as one of the appealing issues in materials science.[1] Specially, concomitant emergence of ferroelectric (FE) and (anti)ferromagnetic orders in a chemically single phase material and strong coupling between these two, termed as magnetoelectric coupling, are extremely promising for future generation of memory devices.[2] Therefore, search for new multiferroic materials, enhanced spontaneous polarization close to room temperature[3] and possible origin of multiferroic order are one of the active areas of research in the field. Current focus mainly involves searching of new materials which have multiferroic orders close to room temperature with significant spontaneous polarizations. Recently, appearance of FE order in few members of RCrO$_3$ series has revived significant attention in this field.[4–10] Hopefully, the results in RCrO$_3$ (R=Lu, Sm, Er, and Gd) clearly demonstrate significantly large magnitude ($\sim \mu$C/cm^{-2}) of electric polarization (P) at reasonably high temperature,[11–13] which is attractive for the technological applications.[14–16]

Recently, the improper ferroelectricity has been argued in few members of RCrO$_3$ where ferroelectricity is suggested to be driven by the magnetic order.[4] However, recent review on RCrO$_3$ clearly demonstrates that onset of FE polar order was observed at much higher temperature for $LuCrO_3$ and $ErCrO_3$.[6] For $LuCrO_3$, the difference between T_N and emergence of polar order as obtained from the pyroelectric current measurement is $\sim$ 80 K.[6,12] Analogous to this scenario, onset of polar order has also been observed around $\sim$ 40 K higher temperature than T_N for $SmCrO_3$.[13] In fact, FE Curie temperature is observed at $\sim$ 27 K higher temperature than T_N. These results open up a fundamental question on whether RCrO$_3$ belongs to the category of genuine improper ferroelectrics?[13] Recently, synchrotron diffraction studies on $SmCrO_3$ confirmed a structural distortion from a centrosymmetric $Pbnm$ structure toward a non-centrosymmetric $Pna2_1$ sub-group at $\sim$ 240 K, around which onset of polar order appeared concomitantly. This result raised an important issue on whether $SmCrO_3$ belonged to the proper or improper ferroelectric class? Careful observations on emergence of FE polar order in RCrO$_3$ demonstrate that onset of polar order always appears at significantly higher temperature than T_N. This motivates us to investigate multiferroic order in an unexplored compound $HoCrO_3$, a member of the RCrO$_3$ series.

In this study we observe another paradigm of FE polar order of $HoCrO_3$ in polycrystalline bulk and film geometry. The results also demonstrate that onset of polar order appears at much higher temperature ($\sim$ 240 K) than T_N (142 K) for polycrystalline specimen analogous to that observed in all the members of RCrO$_3$. The value of electric polarization is reasonably high ~ 0.32 μ C/cm^2 at 10 K. Although T_N shifts toward lower temperature at 132 K for film, polar order still emerges at higher temperature than T_N. The values of FE Curie temperature are found to be close to T_N for both the polycrystalline and film specimens. The polarization vs. applied electric field ($P-E$) loops are measured for both bulk and film recorded at 80 and 180 K, the representative temperatures below and above T_N, respectively. Signature of remanent polarization above T_N is intriguing and attracts the community for further investigation on the origin of polar order in RCrO$_3$.

† Electronic Supplementary Information (ESI) available: AFM image, schematic representation of electric connection for $P-E$ loop measurements in film, fit of the x-ray diffraction pattern at 80 K using Rietveld refinement and details of the refined structural parameters.

[a] *Department of Solid State Physics, Indian Association for the Cultivation of Science, Jadavpur, Kolkata 700 032, INDIA*
∗ Corresponding author's E-mail: sspsg2@iacs.res.in

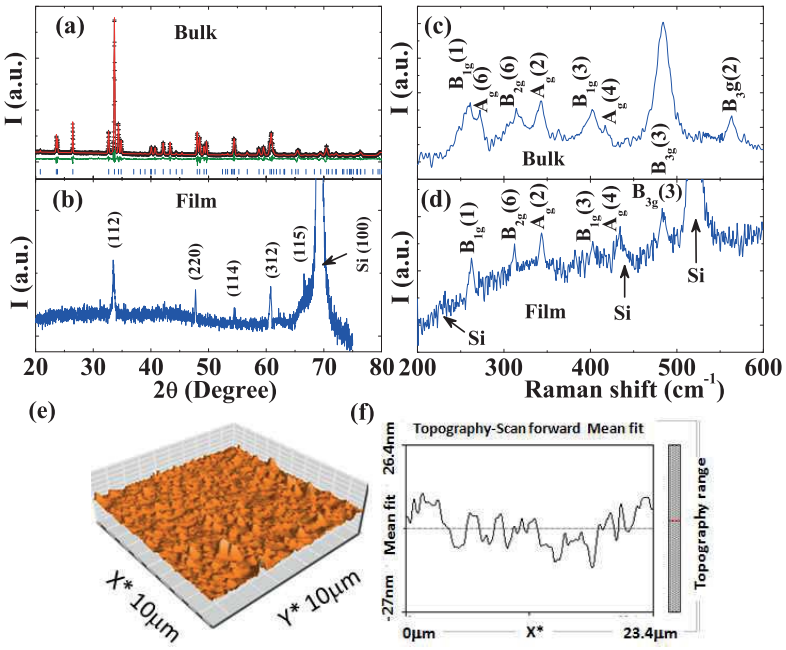

Fig. 1 (Color online) Powder x-ray diffraction data (black symbol) of $HoCrO_3$ with the Rietveld refinement (red line) for bulk (a) and for film (b) with indexing of (*hkl*). Raman spectra for bulk (c) and film (d). The three-dimensional AFM image (e) and a surface topography scan (f).

Analysis of the x-ray diffraction pattern at 160 K reveals the non-centrosymmetric $Pna2_1$ structure which is a sub-group of centrosymmetric *Pbnm* structure appeared at room temperature. The structural analysis suggest that polar octahedral rotations along with Ho atom displacement engineer occurrence of polar order in $HoCrO_3$. Emergence of polar order at much higher temperature than T_N and concomitant appearance of T_N and FE Curie temperature for both polycrystalline and film specimens indicate atypical multiferroic orders in $HoCrO_3$.

2 Experimental

2.1 Synthesis

Polycrystalline $HoCrO_3$ is prepared using solid state reaction of stoichiometric quantities of Ho_2O_3 and Cr_2O_3 at 1673 K for 12 hours followed by several intermittent grinding and heating.[13] As prepared polycrystalline $HoCrO_3$ is used as a target for film synthesis on a Si(100) substrate using pulsed laser deposition (PLD) technique. The energy of laser (Model No: CompexPro 205 F, KrF) is set to 100 mJ (wave length 248 nm). Target to substrate distance is set to 10 cm. Substrate temperature is maintained at 600 ^{0}C. The repetition rate and number of laser pulses are 10 Hz and 40 000, respectively. Base pressure is achieved at $\sim 10^{-4}$ mTorr and during deposition oxygen pressure of the PLD chamber (Neocera, USA) is maintained at $\sim$ 50 mTorr.

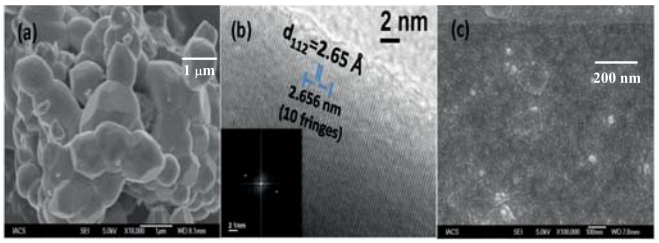

Fig. 2 (Color online) (a) SEM micrograph of polycrystalline $HoCrO_3$ with prominent grain and grain boundary. (b) Lattice fringe pattern as obtained from a high resolution transmission electron micrograph of a particle. The inset shows the corresponding electron diffraction pattern. (c) SEM image of film surface.

2.2 Characterization

Powder x-ray diffraction studies are carried out in a Bruker AXS: D8 Advance diffractometer at room and in a Rigaku TTRAX II x-ray diffractometer for low temperature study, using Cu Kα radiation. Atomic Force Microscope (AFM) image is recorded using Veeco-diCP II. Raman spectra are obtained in a back scattering geometry using a Triple Raman spectrom-

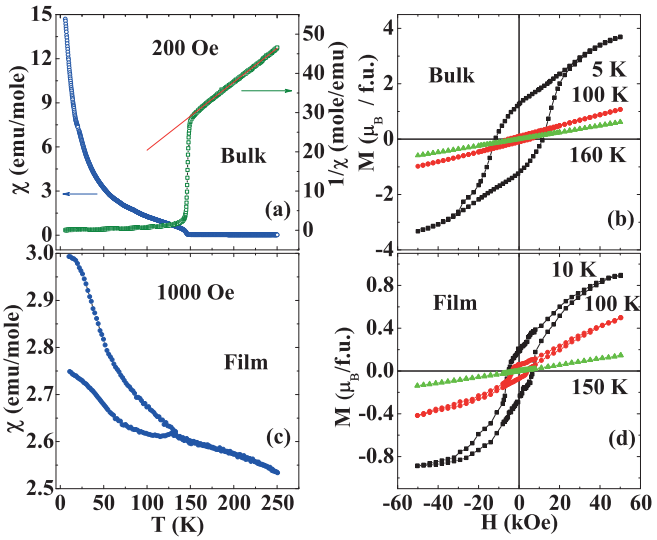

Fig. 3 (Color online) Thermal variation of susceptibility (χ) for bulk (a) and for film (c). Thermal variation of χ^{-1} is also given in (a) with the linear fit using Curie-Weiss behavior as indicated by the straight line. Magnetic hysteresis loops at selective temperatures for bulk (b) and film (d).

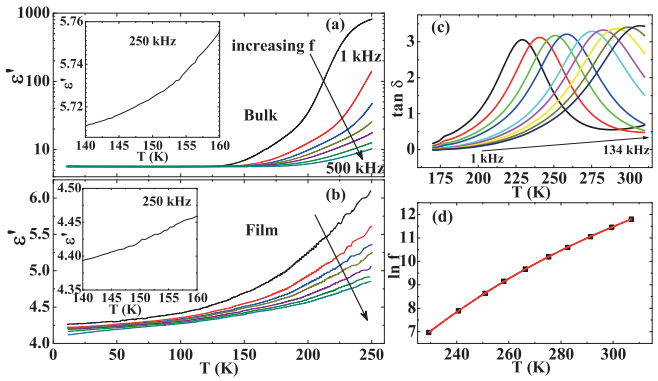

Fig. 4 (Color online) Thermal (T) variation of real component of dielectric permittivity (ε') at various f for bulk (a) and film (b). The corresponding insets absence of any convincing signature around ferroelectric and antiferromagnetic transitions. (c) T variation of $\tan\delta$ recorded at different f. (d) Plot of ln f with T satisfying VF law.

eter (J-Y Horiba, Model No. T64000) with 514 nm wavelength and power density of 2 mWcm^{-2}. **The particle size and morphology are studied in a Scanning Electron Microscope (SEM), model JSM-6700 F, JEOL. Lattice fringes and electron diffraction pattern on a single particle is photographed in a High Resolution Transmission Electron Microscope (HRTEM) of model JEOL, 2010.** For recording electric polarization only perpendicular to the substrate (Fig. S1 of ESI), initially gold is coated on the Si substrate using a gold coater (Eiko IB-2 Ion coater, Japan) on which $HoCrO_3$ film is deposited. An air drying silver paste is used for the electrical contacts. Dielectric permittivity is measured using an E4980A LCR meter (Agilent Technologies, USA). For pyroelectric current (I_p) measurement specimens are cooled down to $\sim$ 5 K in a suitable poling field and then is short circuited at 5 K for nearly one hour before the measurement of I_p in the warming mode. The I_p is recorded in an electrometer (Keithley, model 6517B) and integrated with time for obtaining electric polarization (P). The $P-E$ loops are measured in a FE loop tracer of Radiant Technology, USA which is fitted with a home built liquid N_2 cryostat. The dc magnetization is measured in a commercial magnetometer of Quantum Design (MPMS, evercool). In case of zero-field cooled (ZFC) mode sample is cooled in zero-field and measurement is carried out in the warming mode. For field-cooled (FC) mode sample is cooled in a static magnetic field and measurement is carried out like a ZFC measurement.

3 Results and discussions

3.1 Structural properties

Powder x-ray diffraction pattern recorded at room temperature is depicted in Fig. 1a for bulk. The diffraction pattern is indexed unambiguously using Rietveld refinement. The satisfactory fit is displayed in Fig. 1a by the red curve which confirms that the compound crystallizes in the orthorhombic perovskite structure with the *Pbnm* space group. Bars in the figure represent the diffraction positions. The difference plot given at the bottom ensures a reliable fit of the experimental data. This demonstrates absence of any unidentified line ensuring the high purity of the sample. The reasonable reliability parameters, $R_w \sim 5.79$, $R_{exp} \sim 1.36$, and $\chi^2 \sim 18.08$, indicate the authenticity of the refinement. The position coordinates of Ho, Cr, and O as obtained from the refinement are given in Table S1 of ESI. The lattice constants as obtained from the refinement are a = 5.2517(2) Å, b = 5.5206(2) Å, and c = 7.5467(2) Å, respectively. The values match reasonably with the reported results.[17] X-ray diffraction pattern of the film deposited on Si(100) is depicted in Fig. 1b. All the diffraction peaks could be assigned which correspond to the planes as observed in the bulk counterpart and Si(100) substrate. The peak positions roughly provide the lattice constants as $a \approx 5.24$ Å, $b \approx 5.57$ Å, and $c \approx 7.45$ Å. The value of a is significantly smaller than the value of a (5.43 Å) for Si substrate. The mismatch of a between sample and substrate provides significant tensile strain at the interface defined as,[18] $\eta = (a_{substrate} - a_{sample})/a_{substrate}$. The value of η is $\sim$ 3.5 %.

Raman spectra of both the bulk and film are displayed in Figs. 1c and 1d, respectively. The spectrum for bulk repro-

duces the reported results.[19–21] Different modes of the spectrum are depicted in the figures for both the bulk and film. For film, additional modes are shown which corresponds to the Si substrate as assigned in the figure. The relative shift of the Raman mode of film with respect to bulk roughly provides a film thickness.[22] Here, the average shift provides $\sim$ 160 nm film thickness. Three dimensional AFM image is depicted in Fig. 1e. The surface topography of the film is also shown in Fig. 1f which gives maximum roughness up to $\sim$ 13 nm. Extended AFM image is given in Fig. S1 of ESI.

The SEM micrograph shown in Fig. 2a demonstrates prominent grains and grain boundaries. Average grain sizes are $\sim \mu$m size. The HRTEM image confirms absence of any impurity phase at the grain boundary region and further illustrates the planes extended until the grain boundary region as depicted in Fig. 2b. The d-spacing, as obtained from the lattice fringes, is 2.65 Å, which corresponds to the most intense peak (112) in the x-ray diffraction pattern. Inset shows the corresponding electron diffraction pattern. Fig. 2c shows SEM micrograph for the $HoCrO_3$ film. Top structure, as evident in the AFM image, is also observed in the SEM image.

3.2 Magnetic properties

Thermal variation of ZFC susceptibility (χ_{ZFC}) measured at 200 Oe is shown in Fig. 3a for bulk. Thermal variation of χ^{-1}_{ZFC} is also plotted in the same figure which demonstrates that the plot deviates from Curie-Weiss (CW) behavior below $\sim$ 155 K followed by a sharp fall of χ^{-1}_{ZFC} with T_N at 142 K, in accordance with the reported results.[17,23] Linear χ^{-1}_{ZFC} plot provides paramagnetic moment, $\mu_{eff} \approx 10.98\ \mu_B$ and CW temperature, $\Theta \approx 18.2$ K. The value of μ_{eff} is close to the theoretical value ($\sim 11.55\ \mu_B$) for $HoCrO_3$. Neutron diffraction studies proposed an antiferromagnetic order of Cr^{3+} ions below T_N followed by the Ho^{3+} order with a strong Ho-Cr hybridyzation.[24–26] The χ_{ZFC} and χ_{FC} recorded with 1 kOe in ZFC and FC protocols, respectively are depicted in Fig. 3c for film. The χ_{ZFC} and χ_{FC} deviate from each other below T_N, which is shifted toward low temperature around $\sim$ 130 K compared to the bulk counterpart. Magnetic hysteresis loops are measured at selective temperatures for both bulk and film, which are depicted in Figs. 3b and 3d, respectively. Below T_N, coercivity (H_C) emerges and it increases with decreasing temperature for both, although the values of magnetization and H_C are significantly lower for the film than the bulk counterpart. **We note that value of magnetization is considerably lower in magnitude than the results for the polycrystalline compound. Large disordered surface and interface spins for the film, as also observed for nanocrystalline compound with large surface spins,[27] may give rise to the much smaller value.**

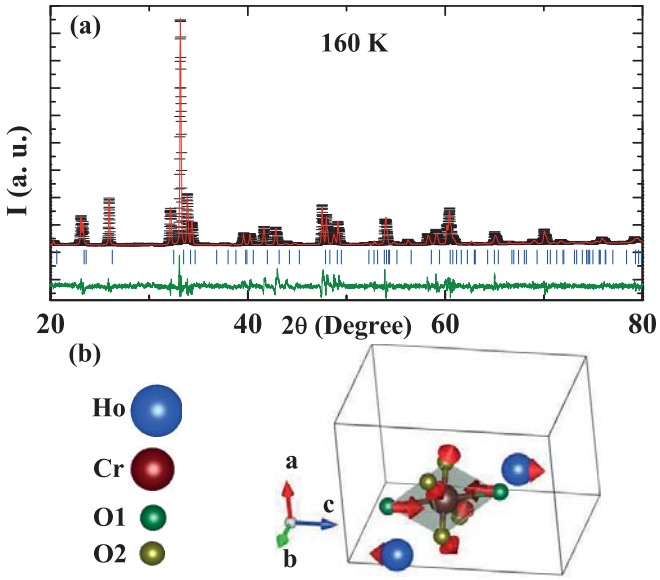

Fig. 6 (Color online) (a) X-ray diffraction pattern at 160 K with the Rietveld refinement as shown by the continuous curve. (b) Displacements of oxygen and Ho atoms, as indicated by the arrows, around a CrO_6 octahedron for structural transformation from *Pbnm* to $Pna2_1$.

3.3 Dielectric properties

The real part of dielectric constants (ε') recorded with temperature at selective driving frequencies (f) are depicted in Figs. 4a and 4b for bulk and film, respectively. For bulk, the ε' displays a high value $\sim$ 1000 close to room temperature at f = 1 kHz and it exhibits the sharp fall with decreasing temperature. The high-ε' above $\sim$ 130 K perhaps ascribes to the extrinsic grain boundary and sample-electrode interface effects **(see Cole-Cole plot in ESI)**.[29] Below $\sim$ 130 K, it shows nearly f and T independent behavior. The significant decrease of ε' is also observed with decreasing temperature from 250 K which is followed by the slow decrease below $\sim$ **125 K** down to 10 K for film. Insets of both the figures display absence of any convincing signature at T_N and at FE ordering temperature as evident in Fig. 5a-d. This is analogous to that observed for $LuCrO_3$ and $ErCrO_3$ where any convincing signature was absent at T_N and FE ordering.[4,12]

The loss tangent component ($\tan\delta$) plotted with temperature (T) is depicted in Fig. 4c for $T > 170$ K over 1−134 kHz frequency (f) range. The peak (T_p) observed in $\tan\delta(T)$ shifts toward high-T region with increasing f. We carefully note that the f-dependence of T_p fails to satisfy Arrhenius law. However, the f-dependence can be satisfactorily analyzed by Vogel Fulcher (VF) law defined as, $f(T_p) = f_0 \exp[E/\{k_B(T_p - T_g)\}]$, where f_0 is the attempt frequency,

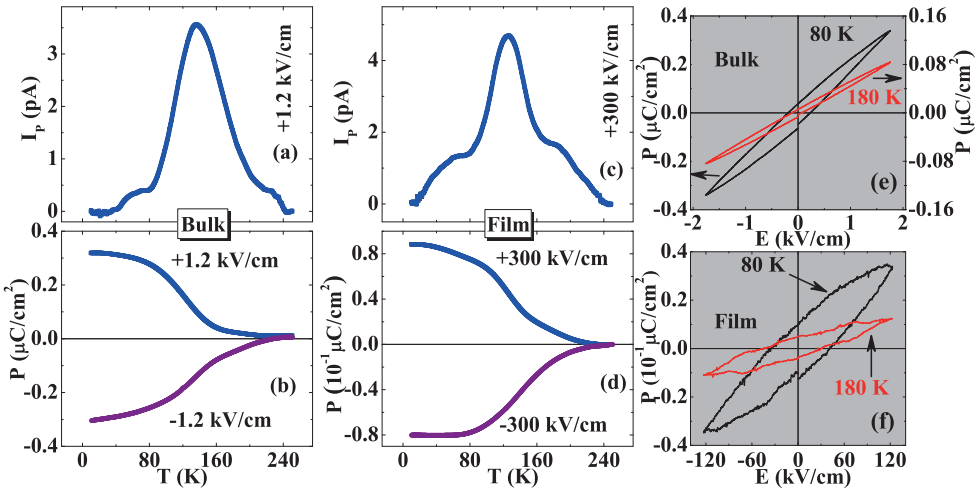

Fig. 5 (Color online) Thermal variation of pyroelectric current (I_p) for bulk (a) and film (c) with poling fields +1.2 and +300 kV/cm, respectively. The corresponding integrated electric polarization (P) for bulk (b) and film (d) both for the positive and negative poling fields. The $P-E$ hysteresis loops at 80 and 180 K for bulk (e) and film (f).

E is the activation energy and T_g is the glassy freezing temperature. The satisfactory fit is depicted in Fig. 4d which provides T_g = 114.1 K, f_0 = 7.2 $\times 10^8$ Hz and E = 9.8 meV. The agreement of the f-dependence of T_p with the VF law signifies glassy freezing.[28–30]

3.4 Emergence of polar order

The FE order in $HoCrO_3$ is revealed for both the bulk and film by measuring I_p at a constant temperature sweep rate of 4.0 K/min. Temperature variations of I_p are recorded after poling at $\pm$ 1.2 and $\pm$ 300 kV/cm for bulk and film, respectively. The I_p at positive poling fields are depicted in Figs. 5a and 5c for bulk and film, respectively. The peaks observed in both the cases are close to T_N. However, analogous to that observed in other members of $RCrO_3$ series,[6,13] onset of FE order emerges at higher temperature than T_N. These are evident in the thermal variations of the spontaneous electric polarization (P) as shown in Figs. 5b and 5d for bulk and film, respectively. The change in P (ΔP) decreases slowly and P vanishes around $\sim$ 240 K ($> T_N$). We note that the ΔP changes the sign while poling in negative electric field and demonstrates switching of polarization. In order to confirm it further, we measure FE hysteresis loops both for bulk and film. For film, electrical connections are done perpendicular to the film surface as depicted in Fig. S2 of ESI. The FE loops recorded at 80 ($< T_N$) and 180 ($> T_N$) K are shown in Fig. 5e for bulk. The P value and remanence of electric polarization decreases considerably at 180 K compared to the values at 80 K. Nevertheless, signature of loop at 180 K is significant and consistent with the non-zero small I_p above T_N. Similar results with nearly $\sim 10^{-1}$ times lower value of P are observed for the film as depicted in Fig. 5f. **Large disordered surface and interface molecules, as well as trapped charge carriers significantly influence the dipolar ordering process, which may result in the significant decrease of polarization value for film.**[31,32] Signature of $P-E$ loop in both the cases is significant and reveals that survival of polar order above T_N which brings out a fundamental issue on the origin of ferroelectricity in $HoCrO_3$.

3.5 Possible origin of polar order and structural correlation

Recent investigation of synchrotron diffraction studies on $SmCrO_3$ over a wide temperature range revealed a structural transition from high temperature centrosymmetric *Pbnm* space group to the low temperature non-centrosymmetric $Pna2_1$ space group close to the onset of polar order.[13] The polar octahedral rotation and Sm displacement have been correlated to the occurrence of ferroelectricity in $SmCrO_3$. Recent reviews on possible origin of various ferroelectric order suggest a new class of ferroelectricity, which neither belongs to proper ferroelectricity, nor to the improper ferroelectricity.[33] To address this issue, Benedek *et al.* proposed oxygen octahedral rotation driven ferroelectricity, a new class of hybrid improper ferroelectricity, where octahedral rotation tunes structural, magnetic, orbital and electrinic degrees of freedom.[33]

To understand structural correlation to the occurrence of polar order we record powder x-ray diffraction patterns below (at 80 K) and above (at 160 K) T_N. X-ray diffraction pattern at 160 K is depicted in Fig. 6a. The satisfactory fit using Rietveld refinement of the diffraction pattern considering $Pna2_1$

space group is shown by the continuous curve. The atomic positions as obtained from the refinement are given in the Table S1 of ESI. The lattice constants are refined as $a \approx 5.2410(1)$ Å, $b \approx 5.5089(2)$ Å, and $c \approx 7.5310(2)$ Å. Satisfactory fit is further indicated by the reliable paramaters with $R_w(\%) \approx 7.73$ and $R_{exp}(\%) \approx 3.54$. We note that refinement of the diffraction pattern at room temperature is satisfactorily performed using *Pbnm* space group in accordance with the reported results for other orthochromates,[4–10] while $Pna2_1$ space group fits the diffraction pattern at 160 K satisfactorily during refinement. At 80 K the satisfactory refinement using $Pna2_1$ space group is shown in Fig. S3 of ESI. Rietveld refinement using non-centrosymmetric $Pna2_1$ space group at low temperature is significant, because emergence of polar order in the current observation is correlated with the structural transformation from centrosymmetric *Pbnm* to non-centrosymmetric $Pna2_1$ structure as also reported in other member, $SmCrO_3$ of the orthochromate series.[13] As indicated by the arrows the displacements of oxygen and Ho atoms around a CrO_6 octahedron are demonstrated in Fig. 6b for a transformation to $Pna2_1$ from *Pbnm* space group where oxygen displacements involves rotation of the octahedron. Thus analogous to that proposed in $SmCrO_3$, structural distortion in non-centrosymmetric $Pna2_1$ space group also causes ferroelectricity in $HoCrO_3$.

The distortion of polar $Pna2_1$ structure can be decomposed by two modes corresponding to the irreducible representations of non-polar GM1+ and polar GM4-, where GM4- is the primary order parameter.[34,35] We note that $Pna2_1$ space group is an isotropy subgroup of *Pbnm*. There, ferroelectricity driven by this structural transition is not a typical case of proper ferroelectrics. Rather, this transition, associated with the oxygen octahedral rotations and Ho displacements, demonstrate analogous scenario as suggested by Benedek *et al.* proposing a new class of ferroelectrics.[33] More experimental verifications with new paradigms are required to establish this new class of ferroelectrics.

4 Conclusions

In conclusion, ferroelectricity is observed in antiferromagnetic $HoCrO_3$ for both in bulk and film geometry. Magnitude of spontaneous electric polarization is reasonably large for polycrystalline specimen. In accordance with the other members of $RCrO_3$ series, onset of polar order appears at much higher temperature ($\sim$ 240 K) than T_N. Structural analysis proposes that the polar oxygen octahedral rotations along with the Ho displacements in the non-centrosymmetric $Pna2_1$ space group engineers ferroelectricity in $HoCrO_3$. Emergence of polar order at much higher temperature than T_N and occurrence of ferroelectric Curie temperature close to T_N for $HoCrO_3$ both in polycrystalline and film geometry attracts the community for the atypical multiferroic behaviour.

Acknowledgment

S.G. acknowledges Nanoscience unit of IACS, Kolkata for using the PLD unit. K.D. wishes to thank CSIR, India for SRF.

References

1 C. N. R. Rao and C. R. Serrao, *J. Mater. Chem.*, 2007, **17**, 4931.
2 J. F. Scott, *J. Mater. Chem.*, 2012, **22**, 4567.
3 J. Young, A. Stroppa, S. Picozzi and J. M. Rondinelli, *Dalton Trans.*, 2015, DOI: 10.1039/c4dt03521f.
4 R. Saha, A. Sundaresan and C. N. R. Rao, *Mater. Horiz.*, 2014, **1**, 20.
5 J. R. Sahu, C. R. Serrao, N. Ray, U. V. Waghmare, and C. N. R. Rao, *J. Mater. Chem.*, 2007, **17**, 42.
6 K. R. S. Preethi Meher, C. Martin, V. Caignaert, F. Damay, and A. Maignan, *Chem. Mater.*, 2014, **26**, 830.
7 G. V. Subba Rao, G. V. Chandrashekhar, and C. N. R. Rao, *Solid State Commun.*, 1968, **6**, 177.
8 T. Yamaguchi and K. Tsushima, *Phys. Rev. B*, 1973, **8**, 5187.
9 C. R. Serrao, A. K. Kunda, S. B. Krupanidhi, U. V. Waghmare, and C. N. R. Rao, *Phys. Rev. B*, 2005, **72**, 220101(R).
10 P. Gupta and P. Poddar, *Rsc. Adv.*, 2015, **5**, 10094.
11 B. Rajeswaran, D. I. Khomskii, A. K. Zvezdin, C. N. R. Rao, and A. Sundaresan, *Phys. Rev. B*, 2012, **86**, 214409.
12 K. R. S. Preethi Meher, A. Wahl, A. Maignan, C. Martin, and O. I. Lebedev, *Phys. Rev. B*, 2014, **89**, 144401.
13 A. Ghosh, K. Dey, M. Chakraborty, S. Majumdar, and S. Giri, *Europhys. Lett.*, 2014, **107**, 47012.
14 A. Ghosh, K. Dey, Sk. Sabyasachi, A. Karmakar, S. Majumdar, and S. Giri, *Appl. Phys. Lett.*, 2013, **103**, 052412.
15 S. Cherepov, P. K. Amiri, J. G. Alzate, K. Wong, M. Lewis, P. Upadhyaya, J. Nath, M. Bao, A. Bur, T. Wu, G. P. Carman, A. Khitun, and K. L. Wang, *Appl. Phys. Lett.*, 2014, **104**, 082403.
16 C. Wang, K.-J. Jin, Z.-T. Xu, L. Wang, C. Ge, H.-B. Lu, H.-Z. Guo, M. He, and G.-Z. Yang, *Appl. Phys. Lett.*, **98**, 192901.
17 B. Tiwari, M. K. Surendra, and M. S. R. Rao, *J. Phys.: Condens. Matter*, 2013, **25**, 216004.
18 K. Dey, A. Ghosh, P. Modak, A. Indra, S. Majumdar, and S. Giri, *Appl. Phys. Lett.*, 2014, **105**, 142905.
19 M. C. Weber, J. Kreisel, P. A. Thomas, M. Newton, K. Sardar, and R. I. Walton, *Phys. Rev. B*, 2012, **85**, 054303.
20 W. Kaczmarek and I. Mörke, *J. Magn. Magn. Mater.*, 1986, **58**, 91.
21 V. S. Bhadram, D. Swain, R. Dhanya, M. Polentarutti, A. Sundaresan, and C. Narayana, *Materials Research Express*,2014, **1**, 026111.
22 I. D. Wolf, *Semicond. Sci. Technol.*, 1996, **11**, 139.
23 Y. L. Su, J. C. Zhang, L. Li, Z. J. Feng, B. Z. Li, Y. Zhou, and S. X. Cao, *Ferroelectrics*, 2011, **410**, 102.
24 W. C. Koehler, E. O. Wqllan, and M. K. Wilkinson, *Phys. Rev.*, 1960, **118**, 58.
25 N. Shamir, H. Shaked, and S. Shtrikman, *Physica* **90B**, 1977, 211.
26 T. Chatterji, N. Jalarvo, C. M. N. Kumar, Y. Xiao, and Th. Brückel, *J. Phys.: Condens. Matter*, 2013, **25**, 286003.
27 **Sk. Sabyasachi, M. Patra, S. Majumdar, S. Giri, S. Das, V. S. Amaral, O. Iglesias, W. Borghols and T. Chatterji, *Phys. Rev. B*, 2012, 86, 104416.**
28 W. Kleemann, *Ferroelectrics*, 2012, **428**, 64.
29 A. Karmakar, S. Majumdar, S. Banerjee, and S. Giri, *Europhys. Lett.*, 2010, **92**, 57009.
30 A. Karmakar, K. Dey, S. Chatterjee, S. Majumdar, and S. Giri, *Appl. Phys. Lett.*, 2014, **104**, 052906.
31 **H. B. Sharma, H. N. K. Sarma, A. Mansingh, *J. Mat. Sci.*, 1999, 34, 1385.**

32 **X. Liu, Y. Wang, P. V. Lukashev, J. D. Burton, and E. Y. Tsymbal, *Phys. Rev. B*, 2012, 85, 125407.**
33 N. A. Benedek, A. T. Mulder, and C. J. Fennie, *J. Solid State Chem.*, 2012, **195**, 11.
34 D. Orobengoa, C. Capillas, M. I. Aroyo, and J. M. Perez-Mato, *J. Appl. Crystallogr.*, 2009, **42**, 820.
35 B. J. Campbell, H. T. Stokes, D. E. Tanner, and D. M. Hatch, *J. Appl. Crystallogr.*, 2006, **39**, 607.

Table of content Thermal variations of magnetic and electric polarizations with their hysteresis loops and possible structural correlation involving rotation of polar CrO_6 octahedron for occurrence of polar order.